

# Heat transfer and effective thermal conductivity analyses in carbon-based foams for use in thermal protection systems

M Grujic<sup>1\*</sup>, C L Zhao<sup>1</sup>, S B Biggers<sup>1</sup>, J M Kennedy<sup>1</sup>, and D R Morgan<sup>2</sup>

<sup>1</sup>Department of Mechanical Engineering, Program in Materials Science and Engineering, Clemson University, Clemson, South Carolina, USA

<sup>2</sup>Touchstone Research Laboratory, Inc., Triadelphia, West Virginia, USA

*The manuscript was received on 4 May 2005 and was accepted after revision for publication on 19 August 2005.*

DOI: 10.1243/146442005X34485

**Abstract:** The applicability of carbon-based foams as an insulation material in the thermal protection systems (TPSs) of space vehicles is considered using a physical analysis and computer modelling. The heat transfer through the foam is considered through its solid phase and the gas residing in the foam pores via conduction and radiation. As the cellular structure of the foam prevents a large-scale motion of the gas, thermal convection is neglected as a heat transfer mode. The results obtained show that, although the gas-phase conduction and radiation can be ignored at near-room temperatures and at sub-atmospheric pressures, their contributions at high temperatures and at near-atmospheric pressure become very significant. It is also found that one can derive an analytical expression for the effective thermal conductivity (a parameter that combines the contributions of both conduction and radiation) as a function of temperature and pressure. Such an expression is shown to be valid for quite large ranges of temperature, pressure, and insulation thickness and, due to its mathematical simplicity, is very suitable for use in computationally intensive large-scale thermo-mechanical analyses of the entire TPS of a space vehicle.

**Keywords:** thermal protection system, porous materials, carbon foams

## 1 INTRODUCTION

Despite their utmost importance, thermal protection systems (TPSs) for space vehicles are not often in the public view. The general public typically hears about heat shields and shuttle tiles only during manned spacecraft missions, especially if such missions are unsuccessful as in the case of the Columbia shuttle in February 2003. The principal function of a TPS is to keep excessive aerodynamic heat from destroying or damaging a space vehicle and its occupants and cargo.

Four different types of TPSs are generally used on a space vehicle [1]: (i) carbon-carbon composite TPS for the nose cap and leading edges, (ii) rigid porous ceramic tiles for windward and leeward surfaces,

(iii) quilted ceramic blankets, and (iv) organic felt blankets. The last two are used for portions of the leeward surface subjected to the lowest heating rates. The rigid porous ceramic tiles are very effective thermal insulators, but they suffer from a number of shortcomings, primarily (a) they are susceptible to low- and high-velocity impact damage due to their inherently limited strength and toughness and (b) they are hygroscopic and, thus, need to be water-proofed before each launch to minimize water absorption (prior to or during launch, or during re-entry) which compromises the tile's insulation properties. Consequently, typically about 40 000 man-hours of maintenance between the flights is needed to inspect and replace damaged tiles and to water re-proof them. To reduce the cost of launching the payloads to low-earth orbits, new TPS concepts are being considered which entail less between-flight inspection and repair. Among the new, TPSs

\*Corresponding author: 241 Engineering Innovation Building, Clemson, SC 29634-0921, USA.

are the ones based on the use of metallic TPS panels. A typical metallic TPS panel consists of an outer and inner metallic honeycomb-core sandwich panel and a metallic side closure around the perimeter of the panel. The panel is filled with insulation and mechanically attached to the vehicle structure. The insulation filling is typically comprised silica- or alumina-based fibrous insulation, multi-layer filling consisting of alternating stacks of thin gold-coated ceramic/composite foils and fibrous insulation layers, metallic foam (e.g. nickel foam), etc. [1]. Such metallic TPS possesses superior impact resistance relative to that encountered in porous ceramic tiles and does not require waterproofing. In addition, it ensures lower maintenance and life cycle costs of the launch vehicles. Such metallic TPS is currently being considered for thermal protection of most of the windward surface area except for the nose and the leading edges [1].

Recently, a new carbon-based foam called CFOAM<sup>®</sup> was developed which possesses an excellent combination of thermally insulating, mechanical and physical properties [2]. CFOAM<sup>®</sup> is produced by Touchstone Research Laboratory, Ltd. from high sulphur bituminous coal using a proprietary technology and it is available in two principal microstructures: (a) an open-cell, reticulated microstructure and (b) a closed-cell microstructure. CFOAM<sup>®</sup> is currently being considered as insulation filling for the metallic TPS panels and for backside insulation of the carbon-carbon TPS sections of the nose cap and the leading edges.

The objective of this work is to ascertain, through basic physical considerations and computer modelling, the suitability of the CFOAM<sup>®</sup> as a TPS insulating material in space vehicles. To accomplish such a challenging goal, one must understand, on the physical grounds, the phenomenon of heat transport through a porous material such as CFOAM<sup>®</sup>. In general, the transfer of heat through a porous material is quite complex phenomenon, because it typically involves all three standard modes of heat transfer [3]: (a) convection through the gas residing in the foam pores; (b) conduction through both the solid and the gaseous phases of the foam, and (c) radiation of the foam cell wall/ligament surfaces. The relative contributions of these three modes of heat transfer vary as a function of the local conditions of temperature and pressure, and they are also affected by the microstructure of the foam itself. Although it is critical to understand the underlying physics for each of the heat transfer phenomena mentioned above and their roles in controlling thermal response of a foam, it is equally important, when one deals with the design of an entire TPS system, to be able to define an effective thermal conductivity of the foam as a function of the local conditions. Such effective

thermal conductivity can be readily implemented into a large-scale (e.g. finite element) thermo-mechanical analysis of such a TPS or its components. Therefore, the objective of this work is two-fold: (a) to quantify relative contributions of different heat transfer mechanisms in CFOAM<sup>®</sup> under various conditions during a vehicle re-entry and (b) to develop an analytical expression, which can be used to compute the effective thermal conductivity under the given local conditions of temperature and pressure, suitable for incorporation in large-scale analyses of the performance of a TPS system in the space vehicle.

Modelling of the heat transfer through porous foam-like materials has been the subject of intense research over the last few years [4–17]. For the most part, the focus of the prior modelling studies was heat convection and conduction as the mechanisms of heat transport. However, at temperature above approximately 700 K, thermal radiation between foam cell walls/ligaments becomes significant. This is particularly important in the present case in which a TPS panel can experience temperatures as high as 2000 K during the flight of a space vehicle.

Q1

The organization of the paper is as follows. A brief overview of the basic heat transfer mechanisms in a foam-like material, the corresponding governing equations, and the boundary conditions associated with a vehicle re-entry are presented in section 2.1. The effect of foam microstructure on the heat conduction path is discussed in section 2.2. A simple kinetic-theory-based model for heat conduction through the gaseous phase is presented in section 2.3. The computational method used to solve the boundary value problem at hand is briefly discussed in section 2.4. The genetic algorithm optimization method used during derivation of an analytical expression for the effective thermal conductivity is briefly reviewed in section 2.5. The results obtained in this work are presented and discussed in section 3. The main conclusions resulting from this work are summarized in section 4.

## 2 COMPUTATIONAL PROCEDURE

### 2.1 Governing equations – initial and boundary conditions

Heat transfer through the TPS porous CFOAM<sup>®</sup> insulation is treated as a one-dimensional problem in which the heat is transferred by conduction (both through the solid phase of the foam and through the gas residing within the foam porosity) and by radiation. Natural convection is neglected on the ground that the foam structure partitions the gas into small packets and limits a large-scale motion

of the gaseous phase. The heat transfer hence governed by the one-dimensional energy conservation equation is

$$\rho C_p \frac{\partial T}{\partial t} = \frac{\partial}{\partial x} \left( k \frac{\partial T}{\partial x} \right) - \frac{\partial q_r}{\partial x} \quad (1)$$

and by the radiative heat transfer equation for a plane-parallel isotropically scattering, homogeneous, grey (frequency-independent) medium with azimuthal symmetry [3] is

$$\frac{\mu}{\beta} \frac{\partial T}{\partial x} + I = 4(1 - \omega)\sigma T^4 + \frac{\omega}{2} \int_{-1}^1 I d\mu' \quad (2)$$

where  $\rho$  is the foam density,  $C_p$  the solid-phase mass heat capacity,  $k$  the thermal conductivity,  $T$  the temperature,  $t$  the time,  $x$  the spatial coordinate,  $q_r$  the radiant net heat flux,  $\mu = \cos \theta$ ,  $\theta$  an angle between the radiation intensity vector  $I$  and the  $x$ -direction,  $\beta$  the extinction coefficient (a sum of the absorption and scattering coefficients),  $\omega$  the albedo of scattering (a fraction of the incident energy scattered or, equivalently, a ratio of the scattering coefficient and the extinction coefficient), and  $\sigma$  the Stefan–Boltzmann constant ( $5.6704 \times 10^{-8} \text{ W/m}^2 \text{ K}^4$ ).

The radiation model used in this work is highly simplified. This was done to obtain the first-order contribution of heat radiation to the heat transfer through CFOAM<sup>®</sup>. This simple model was deemed justified because a number of radiation parameters for CFOAM<sup>®</sup> are not well established, and had to be set to the values found in other similar carbon-based foams. It should also be noted that the radiation behaviour (e.g. the spectral radiation characteristics) of CFOAM<sup>®</sup> is not well established at the present time. Therefore, it is assumed that CFOAM<sup>®</sup> is radiatively non-selective and the grey-body approximation is used. Once more accurate radiation parameters become available for CFOAM<sup>®</sup>, a new more sophisticated radiative model can be introduced.

Although a mathematical treatment of the simple radiation model can be found in many standard textbooks dealing with thermal radiation [3, 18], a brief mathematical description of this model is presented in this section to help the reader follow the basic construction of the mathematical model for heat transfer through a porous material. Equation (2) is obtained from the radiant power conservation equation, which states that the gradient of the radiation intensity is equal to the net change in the volumetric radiant power density, where the latter has four components: (a) an emission term, (b) an absorption term, (c) an in-scattering term, and (d) an out-scattering term. In equation (2), the second term on

the left-hand side corresponds to a sum of the absorption and out-scattering terms, whereas the two terms on the right-hand side correspond to the emission and in-scattering terms, respectively.

Equation (2) is an integro-differential equation which does not have a closed form solution. Hence, several approximations have been proposed to simplify the solution of this equation. In this work, the so-called *spherical harmonics approximation* initially proposed by Jeans [19] is used, within which the radiative intensity is assumed to be expandable in an infinite series as

$$I = \sum_{m=0}^{\infty} \frac{2m+1}{4\pi} P_m(\mu) \psi_m(x), \quad m = 0, 1, 2, \dots \quad (3)$$

where  $P_m(\mu)$  and  $\psi_m(x)$  are the Legendre polynomials and a set of complimentary unknown functions, respectively.

By taking advantage of orthogonality of the Legendre polynomials and limiting the summation in equation (3) to only the first two terms (the so-called *P<sub>1</sub> approximation*), the following system of two ordinary differential equations is obtained

$$\frac{1}{\beta} \cdot \frac{d\psi_1}{dx} + (1 - \omega)\psi_0 = 4(1 - \omega)\sigma T^4 \quad (4)$$

and

$$\frac{1}{\beta} \cdot \frac{d\psi_0}{dx} + 3\psi_1 = 0 \quad (5)$$

In addition, from the orthogonality condition for  $P_m(\mu)$ , which yields

$$\psi_m(x) = 2\pi \int_{-1}^1 P_m(\mu') I(x, \mu') d\mu' \quad (6)$$

and setting  $P_0(\mu) = 1$  and  $P_1(\mu) = \mu$ , one can define the incident radiation  $G(x)$  as

$$G(x) = \psi_0(x) = \int_{-1}^1 I(x, \mu') d\mu' \quad (7)$$

and the net radiation flux  $q_r(x)$  as

$$q_r(x) = \psi_1(x) = \int_{-1}^1 \mu I(x, \mu') d\mu' \quad (8)$$

Furthermore, by differentiating equation (5) and combining it with equations (4), (6), and (7), the following second-order ordinary differential equation

for incident radiation is obtained

$$\frac{\partial^2 G}{\partial x^2} = 3\beta^2(1 - \omega)(G - 4\sigma T^4) \quad (9)$$

Equations (1) and (9) now represent a coupled system of two differential equations (one partial, Equation (1), and one ordinary, equation (9)) with respect to two unknown functions:  $T(x, t)$  and  $G(x)$ . To complete the definition of the one-dimensional heat transfer problem through a foam-like material, the following initial and boundary conditions are assigned to equation (1)

$$T(x, t = 0) = T_{\text{init}} \quad (10)$$

$$q(x = 0, t) = -k \frac{\partial T}{\partial x} - \frac{1}{3\beta} \frac{\partial G}{\partial x} \quad (\text{inner surface, } x = 0) \quad (11)$$

$$T(x = L, t) = T_{\text{out}}(t) \quad (\text{outer surface, } x = L) \quad (12)$$

where  $T_{\text{init}}$  is the constant initial temperature,  $L$  the total insulation thickness,  $T_{\text{out}}$  the temperature of the outer surfaces given as a function of time, and  $q$  the total flux. The boundary conditions defined by equations (11) and (12) denote that the temperature of the outer surface is controlled by the aerodynamic heating, whereas that of the inner surface is governed by the local zero-flux (adiabatic) condition. The use of the adiabatic condition yields the highest temperatures at the inner surface and, hence, the selection of a minimum thickness of the TPS insulation, to be discussed later, is conservative.

The following boundary conditions for diffuse emitting and reflecting surfaces are assigned to equation (9)

$$\frac{\partial G}{\partial x} = 0 \quad (\text{inner boundary, } x = 0) \quad (13)$$

and

$$G - \frac{2}{3\beta(\varepsilon_{\text{out}}/2 - \varepsilon_{\text{out}})} \cdot \frac{\partial G}{\partial x} = 4\sigma T_{\text{out}}^4 \quad (\text{outer boundary, } x = L) \quad (14)$$

where  $\varepsilon_{\text{out}}$  denotes the emissivity of the outer insulation surface and equation (13) is the special case of equation (14) corresponding to a zero value of the emissivity. The boundary conditions defined in equations (13) and (14) are obtained from the condition that the net radiative heat flux at an insulation surface is a difference between the intensity of inside-the-foam radiation reaching the surface and an emitted radiation intensity from the surface.

A simple schematic of the one-dimensional boundary value problem defined in this section is given in Fig. 1.

## 2.2 Pure-conduction thermal conductivity of the foam

As stated earlier, heat conduction through CFOAM<sup>®</sup> is considered as a combination of heat conduction through the solid phase of the foam and heat conduction through the gas within the pores of the foam. The resulting 'pure-conduction' thermal conductivity,  $k$ , is hence a function of thermal conductivities of the solid phase and the gas. In addition, the foam microstructure affects its pure conduction thermal conductivity. Although this function is generally not known,  $k$  must lie between a lower bound,  $k_{\text{LB}}$  (corresponds to an in-series arrangement of the solid phase and gas relative to the direction of heat conduction), defined as

$$k_{\text{LB}} = \frac{k_{\text{solid}}k_{\text{gas}}}{\varepsilon k_{\text{solid}} + (1 - \varepsilon)k_{\text{gas}}} \quad (15)$$

and an upper bound,  $k_{\text{UB}}$  (corresponds to the assumption that the solid phase and the gas are arranged in a parallel manner with respect to the

$$T_{\text{out}}(t), q_{\text{cond}}(t) = q_{\text{r,in}}(t) - q_{\text{r,out}}(t)$$

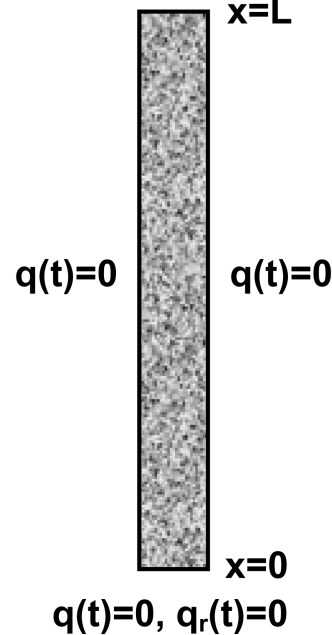


**Fig. 1** A schematic of the one-dimensional boundary value problem associated with heat transfer at a specific location of the TPS of a space vehicle during re-entry. Please refer to the text for an explanation of the symbols

direction of heat conduction), defined as

$$k_{UB} = \varepsilon k_{gas} + (1 - \varepsilon) k_{solid} \quad (16)$$

where  $\varepsilon$  denotes porosity of the foam (a ratio of the porosity volume and the foam volume) and the subscripts solid and gas are used to denote the two constituent phases of the foam. Generally, effective thermal conductivity is defined as weighted sum of its lower and upper bounds as

$$k = (1 - A)k_{LB} + Ak_{UB} \quad (17)$$

where  $A$  is a weighting factor. Following Sullins and Daryabeigi [20–22],  $A$  is set to 1, to ensure a conservative selection of the minimum thickness of the TPS insulation.

Thermal conductivity of the solid phase in a porous material is generally different from that of the same material in the bulk form,  $k_{bulk}$ , due to the fact that the solid phase of a foam consists of thin cell walls or struts whose thickness may become comparable with the phonon mean free path and due to wall/wall (strut/strut) contact resistance contribution to thermal conductivity of the solid phase. It is generally assumed that  $k_{solid} = F(\varepsilon)k_{bulk}$ , where  $F(\varepsilon) = 1$  for  $\varepsilon = 0$  and  $F(\varepsilon)$  decreases continually as  $\varepsilon$  increases. The  $F(\varepsilon)$  function was determined in the present work using an experimental value for thermal conductivity of CFOAM<sup>®</sup> at the room temperature and at the atmospheric pressure.

Based on the analysis presented above, the conduction-only thermal conductivity of the foam can be defined as

$$k = (1 - A) \left[ \frac{Fk_{bulk}k_{gas}}{\varepsilon Fk_{bulk} + (1 - \varepsilon)k_{gas}} \right] + A[\varepsilon k_{gas} + (1 - \varepsilon)Fk_{bulk}] \quad (18)$$

### 2.3 Thermal conductivity of gas

Although thermal conductivity of the bulk solid phase generally shows weak temperature and pressure dependencies, thermal conductivity of the gas is typically a very sensitive function of both temperature and pressure. Following Sullins and Daryabeigi [20–22], thermal conductivity of the gas phase is defined as

$$k_{gas} = \frac{k_{gas,o}}{(\Phi + \Psi)2(2 - \alpha/\alpha)(2\gamma/\gamma + 1)(1/Pr)Kn} \quad (19)$$

where  $k_{gas,o}$  is the temperature-dependent thermal conductivity of the gas phase at the atmospheric pressure,  $\alpha$  a thermal accommodation factor

(a fraction of gas molecules which come into thermal equilibrium with the solid phase during collision with the surface of the solid phase),  $\gamma$  a constant-pressure over constant-volume specific heat ratio,  $Pr$  the Prandtl number, and  $Kn$  the Knudsen number. Parameters  $\Phi$  and  $\Psi$  depend on the gas-phase regime, that is, on the magnitude of the Knudsen number: for  $Kn \leq 0.01$  (i.e. for the continuum regime),  $\Phi = 1$  and  $\Psi = 0$ , and thus  $k_{gas} = k_{gas,o}$ ; for  $0.01 \leq Kn \leq 10$  (i.e. for the transition regime),  $\Phi = 1$  and  $\Psi = 1$ ; and for  $Kn \geq 10$  (i.e. for the free molecular regime),  $\Phi = 0$  and  $\Psi = 1$ .

The Knudsen number is defined as

$$Kn = \frac{\lambda}{\delta} \quad (20)$$

where the gas molecular mean field path,  $\lambda$ , is defined as

$$\lambda = \frac{K_B T}{\sqrt{2}\pi P d_g^2} \quad (21)$$

and the characteristic length scale for gas molecules in a reticulated porous medium,  $\delta$ , is defined as [20]

$$\delta = \frac{\pi D}{4(1 - \varepsilon)} \quad (22)$$

where  $K_B$  is the Boltzmann constant,  $P$  the pressure,  $d_g$  the gas collision diameter, and  $D$  the thickness of the cell wall (strut).

A list of thermophysical parameters for the solid phase in CFOAM<sup>®</sup> and for the gas (air) used in the present work is given in Table 1.

### 2.4 Computational method

The system of two governing non-linear differential equations (equations (1) and (9)) subjected to the initial and boundary conditions, equations (10) to (14), is implemented in the commercial mathematical package FEMLAB [23] and solved for the two dependent variables (temperature and radiation) using the finite element method. The FEMLAB provides a powerful interactive environment for modeling various scientific and engineering problems and for obtaining the solution for the associated (stationary and transient, both linear and non-linear) systems of governing partial differential equations. The FEMLAB is fully integrated with MATLAB, a commercial mathematical and visualization package [24]. As a result, the models developed in the FEMLAB can be saved as MATLAB programs for parametric studies or iterative design optimization. In this work, an optimization algorithm known as the genetic algorithm is implemented in the MATLAB and used to derive an analytical expression

**Table 1** Thermophysical properties of CFOAM<sup>®</sup> and nitrogen gas used in the present work

Property	Symbol	Unit	Value	Equation where first used
CFOAM <sup>®</sup> density	$\rho$	kg/m <sup>3</sup>	270	Equation (1)
CFOAM <sup>®</sup> specific heat	$C_p$	J/kg K	700	Equation (1)
CFOAM <sup>®</sup> thermal conductivity	$(1 - \varepsilon)F(\varepsilon)k_{\text{bulk}}$	W/m K	0.225	Equation (1)
CFOAM <sup>®</sup> emissivity	$\varepsilon_{\text{out}}$	N/A	0.85 <sup>a</sup>	Equation (14)
CFOAM <sup>®</sup> porosity	$\varepsilon$	N/A	0.88	Equation (15)
CFOAM <sup>®</sup> albedo of scattering	$\omega$	N/A	0.8 <sup>b</sup>	Equation (2)
CFOAM <sup>®</sup> extinction coefficient	$\beta$	m <sup>-1</sup>	$(10.23 - 1.77 \times 10^{-3} T)\rho^b$	Equation (4)
CFOAM <sup>®</sup> thickness of the cell wall	$D$	m	$0.014 \times 10^{-3}$	Equation (22)
Collision diameter for nitrogen gas	$d_g$	m	$3.74 \times 10^{-10}$	Equation (21)
Specific heat ratio for nitrogen gas	$\gamma$	N/A	1.4	Equation (19)
Thermal accommodation factor for nitrogen	$\alpha$	N/A	1	Equation (19)
1 atm-pressure thermal conductivity of nitrogen gas	$k_{\text{gas,o}}$	W/m K	$1.3 \times 10^{-11}T^3 - 4.5 \times 10^{-8}T^2 + 9.4 \times 10^{-5}T + 0.0014$	Equation (19)
Prandtl number of nitrogen gas	$P_r$	N/A	$-2.1 \times 10^{-10}T^3 + 5.5 \times 10^{-7}T^2 - 0.00038 T + 0.79$	Equation (19)

<sup>a</sup>The value for emissivity is obtained by setting it equal to that in graphite [18].

<sup>b</sup>Due to a lack of experimental data for the albedo of scattering,  $\omega$ , and for the extinction coefficient,  $\beta$ , the values of these two radiation parameters are set equal to their counterparts in a graphite/epoxy composite [28]. No information is currently available regarding the effect of foam ligament diameter on these two parameters.

Q2

for the effective thermal conductivity of a porous material. Such effective thermal conductivity accounts for heat transfer by both conduction and radiation.

A brief overview of the genetic algorithm is given in the section 2.5.

Standard mesh sensitivity and model robustness analyses are carried out following the procedure outlined in our recent work [25]. The results of these analyses validated that the model developed is mesh-insensitive and robust but the results are not be presented here for brevity.

The governing differential equations, equations (1) and (9), and the boundary conditions, equations (11) to (14), are implemented in FEMLAB using the so-called ‘general form’ for non-linear partial differential equations. Within this approach, the boundary value problem (like the one at hand) is cast into the following forms

$$d_{ij}\dot{u}_j + \nabla \cdot \Gamma_i = F_i \quad \text{over the computational domain, and} \quad (23)$$

$$-n \cdot \Gamma_i = G_i + \frac{\partial R_m}{\partial u_i} v_m \quad \text{the Neumann boundary conditions and/or} \quad (24)$$

$$0 = R_m \quad \text{the Dirichlet boundary conditions} \quad (25)$$

where  $i, j = 1, 2, \dots$  is the number of differential equations in the system,  $u$  are dependent variables, a raised dot is used to denote the time derivative,  $\nabla \cdot$  is a divergence operator,  $d_{ij}$  is a coefficient

matrix,  $\Gamma, F, G$ , and  $R$  are, in general, functions of the spatial coordinates, the dependent variable or space derivatives of the dependent variables, and  $v$  is the Lagrange multiplier. Furthermore,  $\Gamma$  is a flux vector while  $F, G$ , and  $R$  are scalars. In the present case, the two dependent variables are defined as a normalized temperature:  $u_1 = T^* = T/T_0$  and a normalized radiation  $u_2 = G^* = G/4\sigma T_0^4$ , where  $T_0$  is a reference (room) temperature. The boundary value problem defined by equations (1), (9) to (14) is then cast as follows to be consistent with FEMLAB general form

$$\frac{\partial T^*}{\partial t^*} + \frac{\partial}{\partial x^*} \left( k \frac{\partial T^*}{\partial x^*} + \frac{1}{3\beta L(1-\omega)} \frac{\partial G^*}{\partial x^*} \right) = 0 \quad (26)$$

$$\frac{\partial}{\partial x^*} \left( \frac{\partial G^*}{\partial x^*} \right) = 3\beta^2(1-\omega)L^2[G^* - (T^*)^4] \quad (27)$$

$$-k^* \frac{\partial T^*}{\partial x^*} - \frac{1}{3\beta L(1-\omega)} \frac{\partial G^*}{\partial x^*} = 0 \quad \text{at } x^* = 0 \quad (28)$$

$$0 = \frac{T_{\text{out}}(t)}{T_0 - T^*} \quad \text{at } x^* = 1 \quad (29)$$

$$\frac{\partial G^*}{\partial x^*} = 0 \quad \text{at } x^* = 0 \quad (30)$$

$$-\frac{\partial G^*}{\partial x^*} = -\frac{3\beta\varepsilon_{\text{out}}L}{2(2-\varepsilon_{\text{out}})} ((T_{\text{out}}/T_0)^4 - G^*) \quad \text{at } x^* = 1 \quad (31)$$

where  $t^* = 4(1-\omega)\sigma T_0^4/\rho C_p L T_0$  is the normalized time,  $x^* = x/L$  the normalized distance along the insulation thickness, and  $k^* = k/4\sigma T_0^3 L(1-\omega)$  the normalized thermal conductivity.

The solution of equations (26) and (27) subjected to the conditions defined by equations (28) to (31)

gives rise, after conversion to the dimensional quantities, to the variation of  $T$  and  $G$  with  $x$  and  $t$ . These relations at long enough times, combined with equation (10) can be used to determine the steady-state total (conduction plus radiation) heat flux. This value of heat flux combined with the overall through-the-thickness temperature gradient and the Fourier expression for heat flux are next used to determine the effective thermal conductivity of CFOAM<sup>®</sup>. Such 'effective' thermal conductivity combines the contributions of conduction and radiation to the heat transfer through CFOAM<sup>®</sup>.

## 2.5 Genetic algorithm for parameter assessment

The procedure presented in the previous section can be used to compute the effective thermal conductivity at any (mean) temperature and pressure. When one analyses the thermal performance of a TPS panel or such performance of the entire TPS system on a space vehicle during a complete flight (or re-entry) which involves major variations in heat loads and the atmospheric pressure, one generally prefers to have an analytical expression for the effective thermal conductivity as a function of temperature and pressure. Derivation of such expression is given in section 3.2.

In this section, a brief description of the optimization method used to determine the unknown coefficients in an analytical expression for the effective thermal conductivity of a porous material as a function of temperature and pressure is given. The coefficients must be selected so that the deviation of the effective thermal conductivity predicted by such an expression from its counterpart obtained using the finite element procedure described in the previous section is minimal over a wide range of temperatures and pressures.

The question then becomes how to efficiently search the coefficient space for the values which give rise to a global maximum in the objective function (defined as a negative sum of squared differences between the values of the effective thermal conductivity predicted by the analytical expression and by the finite element method).

A review of the literature identifies three main types of search methods: (a) calculus-based; (b) enumerative, and (c) random methods. Despite being very fast, calculus-based methods suffer from two main drawbacks: (i) they are local in scope, that is, they typically locate the maximum which is highest (best) in the neighbourhood of the current search point and (ii) they entail the knowledge of derivatives of the objective function whose evaluation (even through the use of numerical approximations) in

multimodal and potentially discontinuous search spaces represents a serious limitation. In enumerative search methods, values of the objective function are evaluated at every preselected point in the search space, one at a time. These methods generally require evaluation of the objective function at a large number of preselected points, which tends to make them inefficient and not very useful for problems of even moderate size and complexity.

Owing to the aforementioned shortcomings of the calculus-based and enumerative search methods, the genetic algorithm [26], one of the random search methods, is used in this work. A detailed comparison of the code development time and computation time required by the genetic algorithm method and by other calculus-based/enumerative methods was not carried out here. However, we observed that the simplex method (a calculus-based method and our initial choice) did not always give the global optimum.

Through (binary) coding, the genetic algorithm creates a parameter string (a chromosome set) for each considered point (individual) in the search space and uses the Darwinian principle of 'Survival of the Fittest' to ensure that chromosomes of the fittest individuals are retained (with a higher probability) in subsequent generations.

At the beginning of the genetic algorithm search procedure, a random selection of the coefficients is used to create an initial population of individuals (parameter sets) of size  $n$  in the search space. The fitness (i.e. the objective function) is next computed for each individual based on how well each individual performs (in its environment). To generate the next generation of individuals of the same population size, the genetic algorithm performs the following three operations: (1) selection, (2) crossover, and (3) mutation. Within the selection process, individuals who are fit are selected (as parents) for mating, whereas weak individuals die off. Through mating, the parents' create a child with a chromosome set that is some mix of the parents' chromosomes. Mixing of parents' chromosomes during child creation is referred to as crossover. To promote evolution, a small probability is used to enable one or more child's chromosomes to mutate (change). The process of child creation and mutation is continued until an entirely new population (of children) of size  $n$  is generated. The fitness of each child is determined and the processes of selection, crossover, and mutation repeated resulting in increasingly stronger generations of individuals. A logic flow chart of the genetic algorithm is shown in Fig. 2. Few important details about parameter coding, selection, crossover, and mutation are given below.

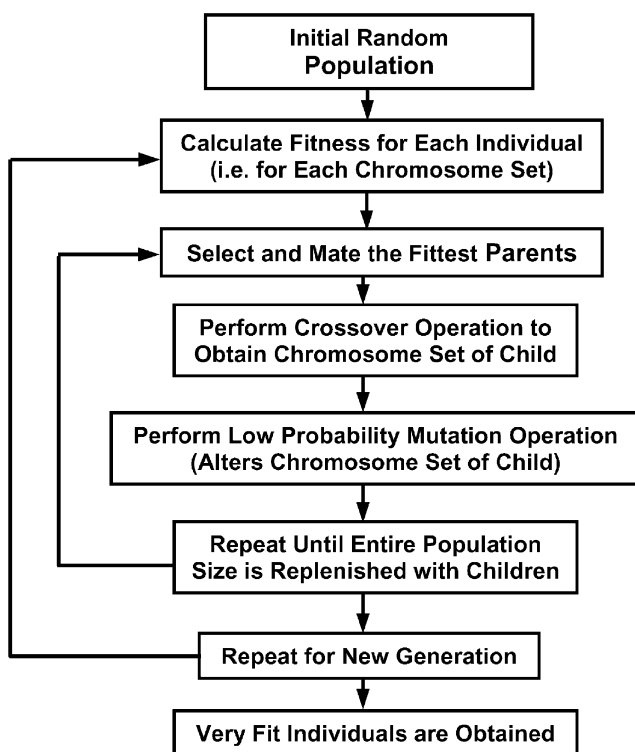


Fig. 2 A genetic algorithm flow chart

### 2.5.1 Binary parameter coding

The total number of possible equally spaced values of each parameter (within the selected range) is first defined. The number of possible values is typically set to  $2^{nm}$ , where  $nm$  is a positive integer. Each possible value of a parameter is next coded using a binary format. For example, when the total number of possible values of a parameter is  $2^{15} = 32\,768$ , that parameter is coded using a string of fifteen 0s and 1s. Binary representations of all the parameters of an individual (a point in the search space) are then attached to form a long string (chromosome set).

### 2.5.2 Tournament selection

Random pairs are selected from the population and the stronger individuals of each pair are allowed to mate and create a child. This process is continued until a new generation of size  $n$  is repopulated.

### 2.5.3 Single-point crossover

Within this process, the chromosome set of the first (stranger) parent (e.g. 10101010) is mapped into that of the child. Then a crossover point is randomly chosen to the right of which the chromosome set of the second parent (e.g. 11001100) overwrites the

chromosome of the first parent, for example. If the crossover point is exactly in the middle of the chromosome, the child's chromosome set for the case at hand is 10101100. The probability for single-point crossover  $P_{\text{cross}}$  is typically set to 0.6. This implies that the probability that the child would retain the entire chromosome set of the first parent is  $1.0 - P_{\text{cross}} = 0.4$ .

### 2.5.4 Uniform crossover

In this case, the crossover can take place at any (and all) points of the parents' chromosome sets and the child can end up with any combination of its parents' chromosomes. The probability for uniform crossover is also typically set to 0.6. It should be noted that, in this case, it is quite unlikely that the child would inherit the entire chromosome set of either of its parents.

### 2.5.5 Jump mutation

In this process, one or more child's chromosomes can mutate and the child can end up with a chromosome not present in either parent. Consequently, the jump mutation can cause one or more parameters to jump from one side of the range to the other. The probability of jump mutation is generally set equal to the inverse of the population size,  $P_{\text{mut}} = 1.0/n$ .

### 2.5.6 Creep mutation

In this type of mutation, the value of one or more child's parameters is changed by a single increment but must remain within the prescribed range. The probability for creep mutation is also typically set equal to the inverse of the population size.

### 2.5.7 Elitism

This operator is used to prevent a random loss of good chromosome strings during evolution. This is accomplished by ensuring that the chromosome set of the best individual generated to date is reproduced. If the best individual is not replicated after the entire population of a new generation is generated through the processes of selection, crossover, and mutation, then the chromosome set of the best individual is mapped into a randomly selected child in the new generation.

The genetic algorithm optimization method discussed here was implemented in MATLAB. Details of this implementation can be found in our previous work [27].

### 3 RESULTS AND DISCUSSION

#### 3.1 Transient analyses

To examine the suitability of CFOAM<sup>®</sup> in TPS applications and determine its minimum thickness required to maintain the temperature of the aluminium space vehicle structure below the maximum acceptable exposure temperature of 450 K, a transient heat transfer analysis defined by equations (1) and (9) to (14) is carried out in this section. Towards that end, the  $T_{\text{out}}(t)$  function in equation (12) is set equal to the time-dependent radiation equilibrium temperature profile at a point on the windward surface for a typical vehicle re-entry trajectory. Such a temperature profile is taken from Ref. [1] and is depicted in Fig. 3. In addition, the pressure profile for the same typical re-entry trajectory of the vehicle as reported in Ref. [1], Fig. 4, is used in the present work. The radiation equilibrium temperature is defined as the temperature of the outer surface which corresponds to the condition when the aerodynamic convection-based input heat flux is balanced by the surface (emission) radiation flux (i.e. it corresponds to the condition in which the conduction flux into the insulation is not considered). The radiation equilibrium temperature, thus, represents the maximum surface temperature for a given input heat flux and for a given surface emissivity.

The results of the present transient heat transfer analysis through a CFOAM<sup>®</sup> insulation during a typical re-entry trajectory of a space vehicle are shown in Fig. 5. For ascertaining the minimum thickness of the CFOAM<sup>®</sup> insulation needed to protect the vehicle's

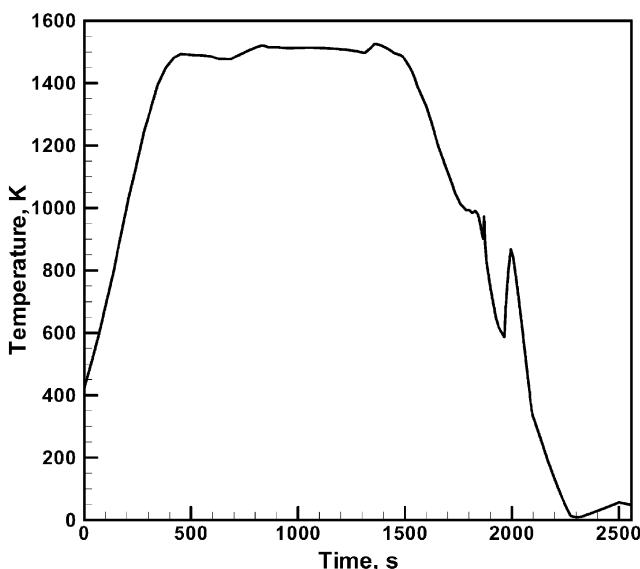


**Fig. 3** A typical radiation equilibrium temperature profile associated with a specific location of the TPS of the space vehicle during re-entry

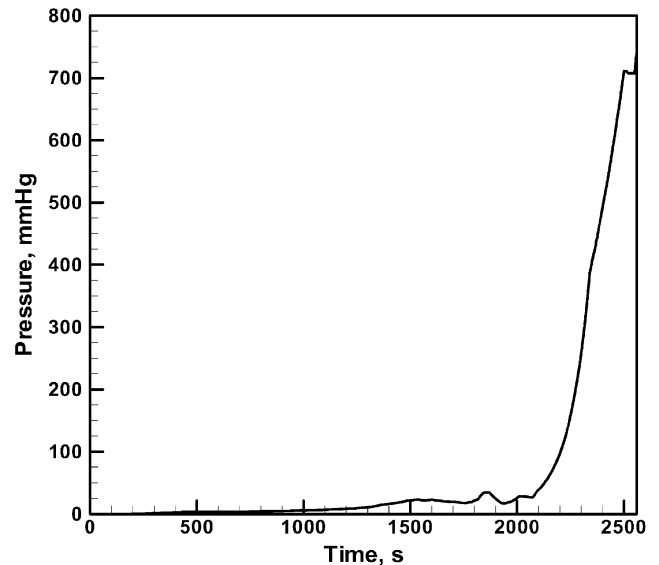


**Fig. 4** A typical pressure profile associated with the re-entry of a space vehicle

aluminium structure, the maximum exposure temperature for the structure (450 K) is also indicated in Fig. 5. The results displayed in Fig. 5, show that a 6-in (152.4 mm) thick insulation is sufficient to maintain the temperature of the bottom surface

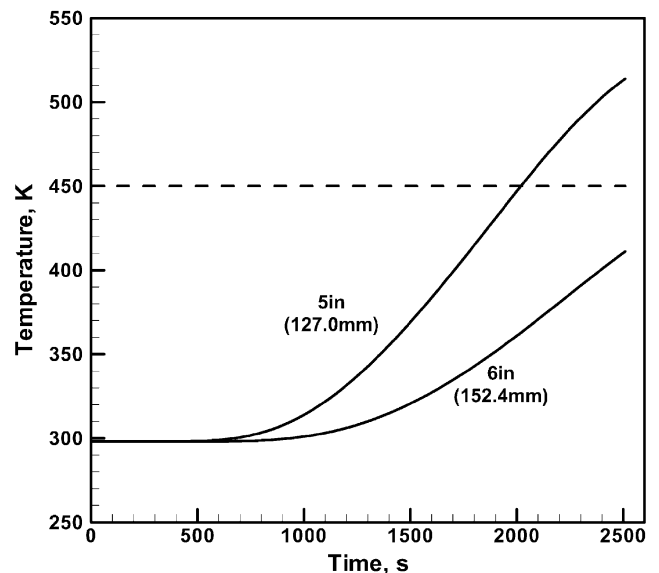


**Fig. 5** Variation of the temperature at the bottom surface of a 5-in (127 mm) and a 6-in (152.4 mm) thick CFOAM<sup>®</sup> insulation during the space vehicle re-entry associated with the temperature and pressure profiles given in Figs 2 and 3, respectively. The maximum allowable exposure temperature (450 K) for the aluminium structure of the vehicle is also indicated

of the insulation below 450 K. A 5-in (127 mm) thick insulation, in contrast, does not meet this design requirement.

Thermal analysis of the performance of various foam-based TPSs is often carried out without consideration of gas conduction or even the heat transfer by radiation. Our model for combined gaseous and solid-phase conduction and radiation heat transfer enables us to quantify the relative contributions of each of the three components of heat transfer. The results of this calculation are displayed in Fig. 6, where a 5-in (127 mm) thick insulation is used. As stated earlier, such insulation is not thick enough to protect the aluminium structure from being exposed to temperature above 450 K when all the three modes of heat transfer are considered (the curve labelled 'All Modes' in Fig. 6).

To suppress radiation as a heat transfer mode, the net radiation heat flux  $q_r$  is set to zero in equation (1), equations (9), (13), and (14) are not considered and the resulting problem is solved using the same finite element approach. The results obtained are shown in Fig. 6, the curve labelled 'Radiation Off' and indicate that if the radiation heat transfer is not considered, the maximum temperature at the bottom surface of the insulation would be under-predicted by approximately 40 K.

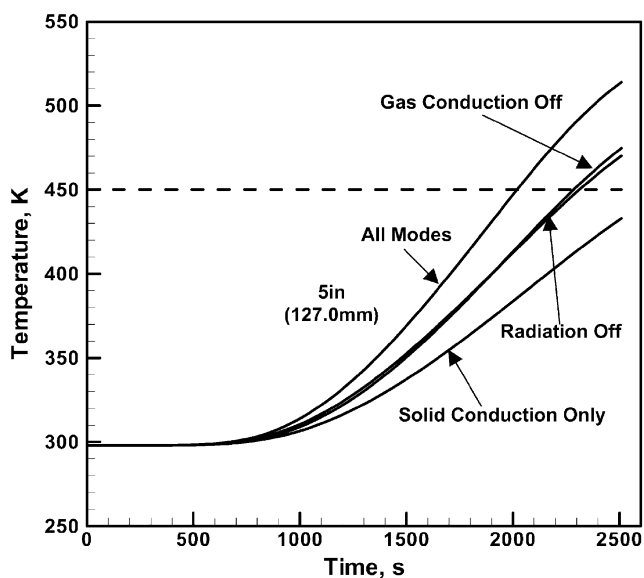


**Fig. 6** Variation of the temperature at the bottom surface of a 5-in (127 mm) thick CFOAM<sup>®</sup> insulation. Labelled curves correspond to the cases when some of the heat transfer modes are not considered to assess their contribution to the overall heat transfer through the insulation. Please see the text for an explanation of the labels

To exclude gas conduction as a heat transfer mode and keep radiation,  $k_{\text{gas,o}}$  is set to zero and equations (1) and (9) to (14) solved. The result of this calculation represented by the curve labelled 'Gas Conduction Off' in Fig. 6 shows that gas conduction also makes a contribution to the heat transfer which is comparable to that of radiation.

If both gas conduction and radiation are excluded, the curve labelled 'Solid Conduction Only' in Fig. 6, the maximum exposure temperature of the aluminium structure is underestimated by as much as 80 K. In fact, one would arrive at a false conclusion that a 5-in (127 mm) thick CFOAM<sup>®</sup> insulation would meet the TPS design requirement that the temperature of the bottom surface remains below 450 K. All these findings suggest that both gas-phase conduction and radiation heat transfer modes must be considered when assessing the performance of porous or foam-like materials such as CFOAM<sup>®</sup> in TPS applications.

### 3.2 Effective thermal conductivity

The heat transfer analysis carried out in this work is one-dimensional in character and it is aimed at assessing the performance of a CFOAM<sup>®</sup>-based TPS at a single point which is located at a portion of the vehicle surface which experiences spatially fairly uniform aerodynamic heating. Under such conditions, the heat flow in the directions parallel with the vehicle surface can be ignored and one can afford to carry out a computationally intensive heat transfer analysis using both the energy conservation equation, equation (1), and the radiative transfer equation, equation (2), and to consider explicitly heat conduction through both the solid phase and the gas. However, when one carries out a thermo-mechanical analysis of an entire section of the space vehicle or of the entire vehicle, one generally prefers an analytical expression which enables evaluation of the effective thermal conductivity as a function of the local conditions of temperature and pressure. If such effective thermal conductivity function is obtained, the heat transfer analysis can be carried out using only equations (1), (10), (11), and (12) in which  $k$  is replaced with an effective thermal conductivity,  $k_{\text{eff}}$ , which includes the effect of both conduction and radiation, and the net radiation heat flux term,  $q_r$ , is set to zero in equation (1).

To compute the effective thermal conductivity of CFOAM<sup>®</sup> as a function of temperature and pressure, the heat transfer problem defined by equations (1) and (9) to (14) is solved under steady-state conditions ( $\partial T/\partial t = 0$ ) in equation (1). In addition, the boundary conditions defined by equations (11) and (12) are changed to read  $T(x=0, t) = T_{\text{in}}$  and

$T(x=L, t) = T_{\text{out}}$ , respectively, where both  $T_{\text{in}}$  and  $T_{\text{out}}$  are constants. Likewise, the first boundary condition for the radiant heat transfer equation, equation (13), is changed to be of the form of equation (14) with  $\varepsilon_{\text{out}}$  and  $T_{\text{out}}$  replaced with  $\varepsilon_{\text{in}}$  and  $T_{\text{in}}$ , respectively. As the problem is now time-independent, the initial condition defined by equation (10) is not considered. To compute the effective thermal conductivity at a given value of  $T$  and  $P$ , a small temperature difference,  $\Delta T = 0.1$  K is applied across the insulation ( $T_{\text{out}} = T + \Delta T/2$ ,  $T_{\text{in}} = T - \Delta T/2$ ), and the computed steady-state heat flux,  $q$ , and  $\Delta T$  used in the following equation

$$k_{\text{eff}} = \frac{q}{\Delta T} \quad (32)$$

The results of this calculation are displayed as a contour plot in Fig. 7 and show that the room-temperature/atmospheric-pressure thermal conductivity of CFOAM<sup>®</sup> reported by Touchstone Research Laboratory Ltd [2] of  $\sim 0.25$  W/m K is reproduced. In addition, the results displayed in Fig. 7 show that increases in both pressure and temperature give rise to an increase in the effective thermal conductivity. The effect of an increase in pressure can be attributed to an increasing role of gas conduction to heat transfer through the porous insulation. An increase in temperature, in contrast, promotes both heat conduction through the gas and heat radiation.

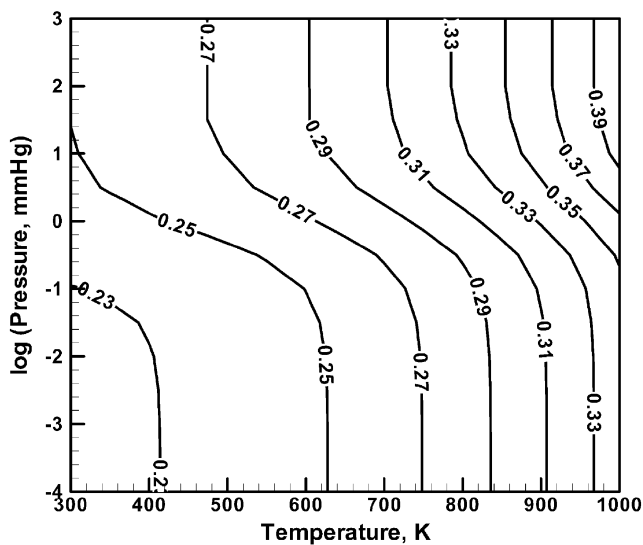


**Fig. 7** The effect of temperature and pressure on the effective thermal conductivity in W/m K of CFOAM<sup>®</sup>. The effective thermal conductivity combines the contributions of conductive and radiative heat transfers through the foam

To further highlight the effect of the pressure, variation of the thermal conductivity with gas pressure at four different temperatures is shown in Fig. 8. This variation clearly delineates the three basic regimes of gas conduction: (a) a rarefied gas (free molecule) regime at the lowest pressures, (b) a transition regime at the intermediate pressures and (c) a continuum regime at the highest pressure. In accordance with equations (19) to (22), thermal conductivity increases linearly with pressure in the rarefied gas regime. In addition, in accordance with equation (19), the effective thermal conduction is pressure-invariant at high pressures (in the continuum gas regime). Pressure levels at which the transition between different regimes takes place appear to be only weakly affected by temperature.

As explained earlier for large-scale thermo-mechanical analyses of a space vehicle or its sections, one prefers an analytical expression for the effective thermal conductivity as a function of temperature and pressure (for a given thickness of the TPS insulation). To derive such an expression, the results displayed in Figs 7 and 8 are fitted to the following functional form

$$k_{\text{eff}} = \frac{C_1 + C_2}{2} + \frac{C_1 - C_2}{\pi} \tan^{-1} (C_3 \log P(\text{mmHg}) + C_4) \quad (33)$$

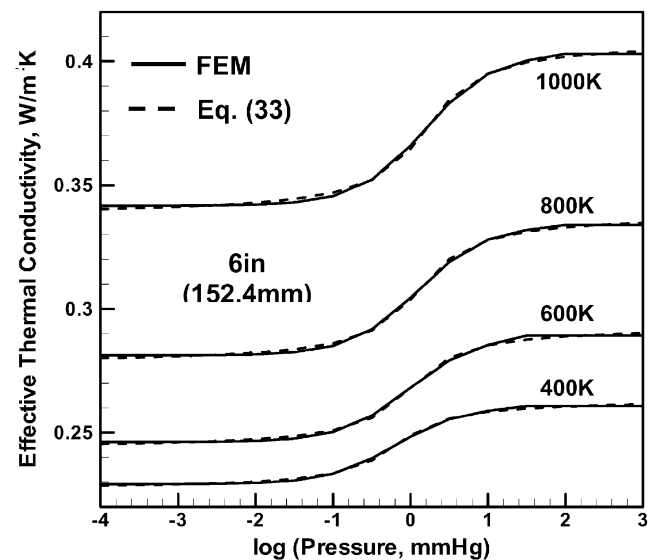


**Fig. 8** The effect of pressure on the effective thermal conductivity of CFOAM<sup>®</sup> at different temperatures. The curves clearly reveal the three gas-phase regimes: a free molecule, low-pressure regime, a transition, intermediate-pressure regime, and a continuum high-pressure regime

where  $C_1$ ,  $C_2$ ,  $C_3$ , and  $C_4$  are quadratic polynomials of temperature.

The functional form given in equation (33) is consistent with the fact that at the high pressure (i.e. in the continuum gas regime),  $k_{\text{eff}}$  is independent of pressure and that at the lowest pressure (the free molecule regime),  $k_{\text{eff}}$  varies linearly with pressure but its rate of change with pressure is very small (approaching zero). The genetic algorithm method described in section 2.5 is used to determine temperature-dependent coefficients  $C_1$ ,  $C_2$ ,  $C_3$ , and  $C_4$ . The results of this procedure for a 6-in (152.4 mm) thick CFOAM<sup>®</sup> insulation can be summarized as follows

$$C_1 = 0.269 - 0.000116T + 2.54 \times 10^{-7}T^2$$

$$C_2 = 0.263 - 0.000198T + 2.72 \times 10^{-7}T^2$$

$$C_3 = 1.76 + 0.000474T - 3.61 \times 10^{-7}T^2$$

$$C_4 = 1.22 - 0.00266T + 1.06 \times 10^{-6}T^2$$

The effective thermal conductivity predicted by equation (33) is displayed in Fig. 8 for comparison with their counterparts obtained using the finite element procedure for a 6-in (152.4 mm) thick CFOAM<sup>®</sup> insulation. The agreement between the two sets of results is quite good over a wide range of pressure and temperature, suggesting that equation (33) can be used to express the functional dependence of the effective thermal conductivity on pressure and temperature.

To test the applicability of equation (33) for insulation with thicknesses different than 6 in (152.4 mm), the transient thermal analysis discussed in the previous section is repeated using both the explicit treatment of gas-phase conduction and radiation, and using the analytical expression for the thermal conduction for a set of insulation thicknesses between 2 (50.8 mm) and 10 in (254.0 mm). The results of this calculation are shown in Fig. 9. It is seen that the analytical expression for thermal conductivity, equation (33), gives a quite reliable prediction of the thermal response of CFOAM<sup>®</sup> over a relatively large range of insulation thicknesses.

It should be noted that the values for the radiation parameters (e.g. the scattering albedo  $\omega$  and the extinction coefficient  $\beta$ ) for the CFOAM<sup>®</sup> listed in Table 1 were not measured but rather guessed using the values of their counterparts in graphite. Therefore, a sensitivity analysis is carried out to determine the effect of variations in these parameters on the calculation results. It is found that  $\pm 50\%$  changes in these parameters give rise to a maximum change in the local temperature

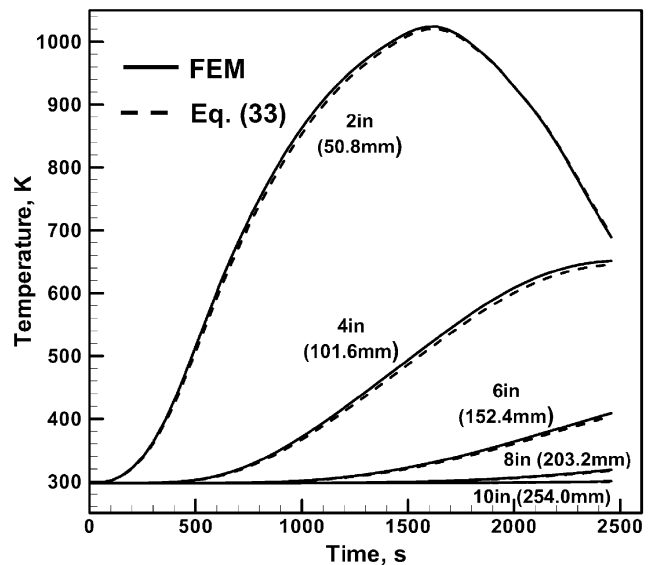


**Fig. 9** Validation of the analytical expression for the effective thermal conductivity of CFOAM<sup>®</sup> as a function of pressure and temperatures, equation (33), for use in the transient heat transfer analyses associated with the re-entry of a space vehicle

by  $\sim 3\%$  and in the local effective thermal conductivity of  $\sim 5\%$ .

## 4 CONCLUSIONS

Based on the results obtained in this work, the following main conclusions can be drawn.

1. Heat conduction through a carbon foam material like CFOAM<sup>®</sup> via gas-phase conduction and radiation is not significant at sub-atmospheric pressures and at near-room temperatures. However, the role of these two modes of heat transfer becomes significant at high temperatures and near-atmospheric pressures.
2. A failure to include heat conduction through the gas phase and radiation during a thermal analysis of the CFOAM<sup>®</sup> insulation during a vehicle re-entry may lead to an underestimation of the minimum insulation thickness required to protect the underlying aluminium structure of the vehicle from being exposed to temperatures exceeding 450 K.
3. It is possible to derive an analytical expression for the effective thermal conductivity (which combines the effects of heat conduction through the solid and gaseous phases and via radiation) as a function of temperature and pressure which is valid over a wide range of insulation thicknesses.

## ACKNOWLEDGEMENTS

This work was sponsored by the US Air Force through Touchstone Research Laboratory, Ltd. The authors acknowledge valuable discussions with Professors Don Beasley, Richard Miller, and Jay Ochterbeck of Clemson University.

## REFERENCES

- Q3
- 1 Blosser, M. *Advanced metallic thermal protection systems for reusable launch vehicles*, PhD dissertation, University of Virginia, May 2000.
  - 2 Morgan, D. R. *Coal based carbon foam for high temperature applications*, MS Thesis, University of North Texas, Denton, Texas, 2001.
  - 3 Ozisik, M. N. *Radiative transfer and interactions with conduction and convection*, 1973 (Wiley).
  - 4 Hunt, M. L. and Tien, C. L. Effects of thermal dispersion on forced convection in fibrous media. *Int. J. Heat Mass Transfer*, 1988, **31**, 301–309.
  - 5 Younis, L. B. and Viskanta, R. Experimental determination of the volumetric heat transfer coefficient between stream of air and ceramic foam. *Int. J. Heat Mass Transfer*, 1993, **36**, 1425–1434.
  - 6 Lee, Y. C., Zhang, W., Xie, H., and Mahajan, R. L. Cooling of a FCHIP package with 100 W, 1 cm<sup>2</sup> chip. In Proceedings of the 1993 ASME International Elec. Packaging Conf., Vol. 1, 1993, pp. 419–423 (ASME, New York).
  - 7 Lu, T. J., Stone, H. A., and Ashby, M. F. Heat transfer in open-celled metal foams. *Acta Mater.*, 1998, **46**, 3619–3635.
  - 8 Lu, T. J. and Chen, C. Thermal transport and fire retardance properties of cellular aluminium alloys. *Acta Mater.*, 1999, **47**, 1469–1485.
  - 9 Calmidi, V. V. and Mahajan, R. L. The effective thermal conductivity of high porosity fibrous metal foams. *ASME J. Heat Transfer*, 1999, **121**, 466–471.
  - 10 Calmidi, V. V. and Mahajan, R. L. Forced convection in high porosity metal foams. *ASME J. Heat Transfer*, 2000, **122**, 557–565.
  - 11 Paek, J. W., Kang, B. H., Kim, S. Y., and Hyun, J. M. Effective thermal conductivity and permeability of aluminium foam materials. *Int. J. Thermophys.*, 2000, **21**, 453–464.
  - 12 Boomsma, K. and Poulikakos, D. On the effective thermal conductivity of a three-dimensionally structured fluidsaturated metal foam. *Int. J. Heat Mass Transfer*, 2001, **44**, 827–836.
  - 13 Boomsma, K. and Poulikakos, D. The effects of compression and pore size variations on the liquid flow characteristics in metal foams. *Trans. ASME J. Fluid Eng.*, 2002, **124**, 263–272.
  - 14 Zhao, C. Y., Kim, T., Lu, T. J., and Hodson, H. P. Modelling on thermal transport in cellular metal foams. In Eighth Joint AIAA/ASME, Thermophysics and Heat Transfer Conference, AIAA 2002-3014, St. Louis, Missouri, USA, June 2002.
  - 15 Zhao, C. Y., Kim, T., Lu, T. J., and Hodson, H. P. Thermal transport in high porosity cellular metal foams. *J. Thermophys. Heat Transfer*, in press.
  - 16 Lu, T. J. Ultralight porous metals: from fundamentals to applications. *Acta Mech. Sinica*, 2002, **18**, 457–479.
  - 17 Kim, T., Fuller, A. J., Hodson, H. P., and Lu, T. J. An experimental study on thermal transport in lightweight metal foams at high Reynolds numbers. In Proceedings of the International Symposium of *Compact Heat Exchangers*, Grenoble, France, 2002, pp. 227–232.
  - 18 Modest, M. F. *Radiative heat transfer*, 2nd edition, 2003 (Academic Press, New York).
  - 19 Jeans, J. H. The equations of radiative transfer of energy. *Int. J. Heat Mass Transfer*, 1965, **8**, 1203–1208.
  - 20 Sullins, A. D. and Daryabeigi, K. Effective thermal conductivity of high porosity open cell nickel foam. AIAA 2001-2819, 11–14 June 2001.
  - 21 Daryabeigi, K. Thermal analysis and design of multi-layer insulation for re-entraerodynamic heating. AIAA 2001-2834, 11–14 June 2001.
  - 22 Daryabeigi, K. *Design of high temperature multi-layer insulation for reusable launch vehicles*, PhD dissertation, University of Virginia, May 2000.
  - 23 FEMLAB 3.0a, 2004 (COMSOL Inc., Burlington, MA, USA). www.comsol.com.
  - 24 MATLAB, 6th edition, The Language of Technical Computing, 2003 (The MathWorks Inc., Natick, MA, USA).
  - 25 Grujicic, M. and Chittajallu, K. M. Design and optimization of polymer electrolyte membrane (PEM) fuel cells. *Appl. Surf. Sci.*, 2004, **227**, 56–72.
  - 26 Goldberg, D. E. *Genetic algorithms in search, optimization and machine learning*, 1989 (Addison-Wesley, Reading, MA).
  - 27 Grujicic, M., Cao, G., and Gersten, B. Optimization of the chemical vapor deposition process for carbon nanotubes fabrication. *Appl. Surf. Sci.*, 2002, **191**, 223–239.
  - 28 Chern, B.-C., Moon, T. J., and Howell, J. R. On-line processing of unidirectional fiber composites using radiative heating: II. Radiative properties, experimental validation and process parameter selection. *J. Composite Mater.*, 2002, **36**(16), 1935–1965.

## APPENDIX

## Notation

$A$	weighting factor
$C_p$	solid-phase mass heat capacity
$d$	gas collision diameter
$D$	thickness of the cell wall (strut)
$G$	incident radiation
$k$	thermal conductivity
$K_B$	Boltzmann's constant
$Kn$	Knudsen number
$P$	pressure
$P_m$	Legendre polynomial of the $m$ th order
$Pr$	Prandtl number
$q$	heat flux
$T$	temperature
$x$	spatial coordinate

$\alpha$	thermal accommodation factor
$\beta$	extinction coefficient
$\delta$	characteristic length scale for gas molecules in the porous medium
$\varepsilon$	porosity
$\varepsilon$	emissivity
$\theta$	angle between the radiation intensity vector $I$ and x-direction
$\lambda$	gas molecular mean field path
$\rho$	foam density
$\sigma$	Stefan-Boltzmann constant

*Subscripts*

o	quantity at atmospheric pressure
r	radiation-related quantity

*Superscripts*

bulk	bulk-solid quantity
g	gas quantity
solid	solid-phase quantity
*	normalized quantity

